CHAPTER 3

MATERIALS AND METHODS

3.1 Morphotectonic Analysis

3.1.1 Structural Trendline

Structural trendlines map is interpreted through IRS P6 LISS IV (2010) and Landsat TM satellite imagery of 2014 (Fig. 4.2, 4.3 and 4.4). The structural trend appear as linear in decipherable tonal contrast in satellite imagery. Structural Trendline is recognized on the basis of tonal boundaries between two major rock units, topographic ridges, related to compositional bending/layering and trains of dark boulders representing dyke. This is in conjuction with contextual factor representing structural/lithology/geomorphology significance. Discretion was used to eliminate non-structural features and only structural features was given priority in the interpretation (Drury et al. 1984; Nair, 1990 and Balaji, 2010).

3.1.2 Lineament Analysis

Lineaments are defined as straight linear elements visible at the Earth's surface and which are the representations of geological and/or geomorphological phenomena (Clark and Wilson, 1994). O'Leary, (1976) defined the lineament as a mappable, simple, or composite linear feature of a surface, whose parts are aligned in rectilinear or slightly curvilinear relationship and which differs distinctly from the patterns of adjacent features. A lineament in satellite imagery and aerial photographs can be noticeable either darker pixels in the middle and lighter on both sides; or is lighter on one side and darker on the other side. Therefore, lineaments are identified by a series of adjacent pixels at the boundary of brightness changes on an image (Shorth, 2004). Lineaments are originated from two types of sources. Firstly, lineaments may occur due to tectonic activity. This kind of lineaments usually corresponds to faults, joints and/or lithological boundaries. The other type of lineaments is due to manmade features including roads, railroads, crop field boundaries or any kids of variations in land use patterns. First type of lineaments, occurred by the tectonic activity, is the main concern of this study.

3.1.2.1 Enhancement Techniques for Lineament Delineation

In order to improve the visual interpretability of an image by increasing the apparent distinction between the features in the scene (Lillesand and Keifer, 1999), some enhancement techniques were used for lineament extraction in this study which are as follows;

- Contrast Enhancement,
- Color Composite,
- Principle Component Analyses (PCA),
- Decorrelation Stretching technique.

3.1.2.2 Methods of Lineament Delineation

In lineament delineation from the remotely sensed data, there are different methods developed by researchers (Wang and Howarth, 1990; Zlatopolsky, 1997; Süzen and Toprak, 1998 and Richetti, 2002). The most widely used techniques are as fallows;

- Manual Lineament Extraction,
- Semi-Automatic Lineament Extraction,
- Automatic Lineament Extraction,

3.1.2.3 Manual Lineament Extraction

In the present studies, Lineament analysis is accomplished by visual interpretation after the enhancement techniques are applied to the image. The lineaments detected during the interpretation process are digitized directly on the image(s) on hard copies or on the screen. The main advantage of the manual extraction is that it is easy to detect the nongeological lineaments such as roads, field boundary or fences with human perception (Kocal et al. 2004).

3.1.2.4 Data Processing and Interpretation

IRS 1D, LISS III (Linear Imaging Self Scanning), FCC (False Colour Composite) satellite imagery of 1998 of wavelength range 0.555 µm to 1.625 µm on 1:25000 scale and Landsat TM 2007 and 2014 of 30m (merged with 15m Panchromatic) spatial

resolution were used for the image processing. Visual interpretation of lineaments/fractures, was done using ENVI 4.5, Erdas Imagine 2011 softwares (Fig. 4.5) and the final digitised thematic maps were done using ArcGIS software 2010. The lineaments were interpreted on the basis of linearity, curvilinearity, vegetational alignment, lithological contact, rectilinearity of the drainages and offsetting of lithology (Brockmann et al. 1977; Bakliwal, 1978; Balaji and Ramasamy, 1993 and Ramasamy and Balaji, 1995). Landsat TM data and the ASTER data are also used for the interpretation of lineaments in this study. The advantage of using ASTER data is that it has radiometric and spectral resolution. It has higher spatial resolution in the visible and near infrared ranges.

3.1.3 Rose Diagram

In structural geology, rose diagrams are used to plot the orientation of lineaments in the present study, Rose diagram is prepared through Rockworks software v.16 to get the lineaments direction and its size (Fig. 4.6). After using image processing techniques, lineaments are digitized in ArcGis software. The aziumuth of the lineaments are calculated using spatial analysis tool of ArcGis and exported to Rockwork software to create and plot Rose Diagram.

3.1.4 Field Investigation – Identification of active faults

Field survey was carried out to collect geological and geomorphological evidences to establish the active tectonics/active faults. After the interpretation of faults from satellite imagery, detailed mapping have been done along the faults. The activeness of the faults are determined based on the geological, geomorphological, geodetic and seismologic indicators. Some of the recognising criteria which are followed are fault displacement and fault scarps, shutter ridge, pressure ridge, piggyback basin, offset streams, open fissures, offset of terraces, sag pond, folding or warping of young alluvial materials and earthquake epicentral distribution.

In addition, evidences were collected on the structural influence on the drainages and the attitude of beds were measured to decipher the structure.

3.2 Morphometric Analysis

3.2.1 Quantitative Geomorphology

The study of the nature of landforms, landscapes, surface processes and their origin is known as geomorphology, which may have either a qualitative or quantitative representation (Morisawa, 1985; Baker, 1986a; Easterbrook, 1999 and Keller and Pinter, 2002). According to Morisawa, (1985), quantitative geomorphology represents a new subfield of geomorphology that is defined as "the application of mathematics and statistical techniques to the study of landforms, their description and the processes by which they are created and changed". Hence, the quantitative measurement and analysis of landforms and topography are the fundamental factors of morphometry (Hayden, 1986 and Keller and Pinter, 2002) or geomorphometry (Summerfield, 1997) that summarize numerical definitions of the Earth's surface shape in correlation with landscape processes. Morphometric analysis is a proven method reliable and relatively accurate in the assessment of tectonic activity of large-scale regional analysis of natural geomorphic forms (Azor et al. 2002; Silva et al. 2003 and Zovoili et al. 2004). In addition, this approach is easy, does not require expensive equipment, and can be remotely performed without conducting field measurements. Morphometric analysis of surface-stream networks has been used to quantitatively describe stream basins with the goal of understanding their processes and evolution (Horton, 1945; Strahler, 1952, 1957, 1958, 1964; Shreve, 1967; Patton and Baker, 1976; Rodrique-Iturbe and Valdes, 1979; Abrahams, 1984; Chutha and Doodge, 1990 and Wilgoose et al.1991).

In the present study, focus is given on the landforms formed by tectonic process.

3.2.2 Drainage Analysis

The drainage network of the South Andaman Island has been interpreted from ASTER DEM satellite imagery of 30 m resolution (Fig. 3.1). The study area is drained by several structurally controlled drainage patterns such as trellis, dendritic, mix radial- annular, parallel and linear drainages. Trellis and dendritic drainages dominate the overall drainage pattern of the study area. Trellis drainage pattern is greatly responsible

for the formation of fractured intermontane valleys, while liner drainage dominates high elevated peaks and coastal cliffs. The study area has dendritic drainage pattern in Ophiolite formations which is a typical character of homogenous rock types. The diversified drainages indicate that Island has diverse structural pattern, geological and hydrological settings and these drainages are said to be reflections of surface and subsurface formations.

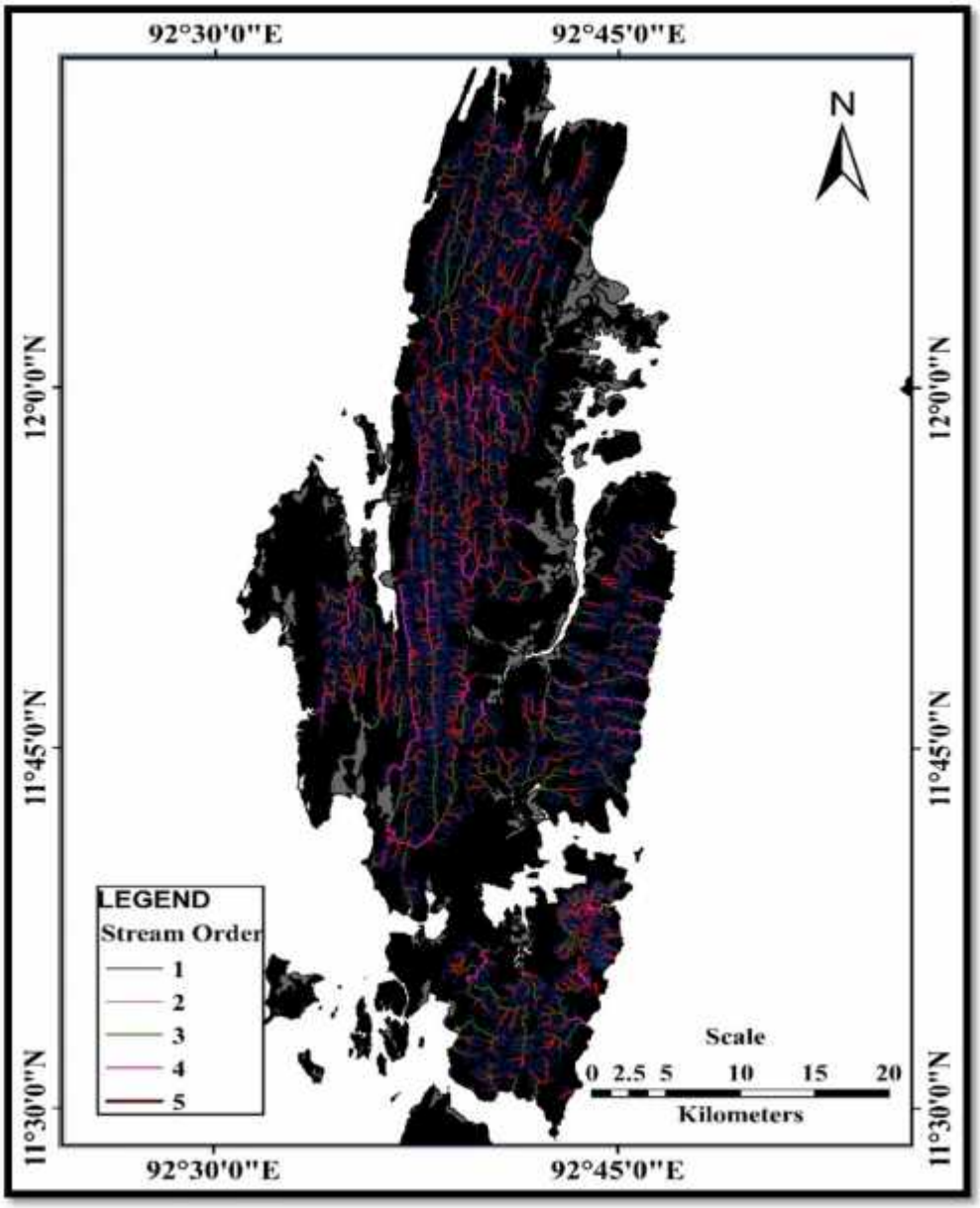

Fig. 3.1 Drainage network and Stream Order of South Andaman Island interpreted from ASTER DEM Satellite imagery.

3.2.3 Mountain front sinuosity index (Smf)

Mountain fronts are defined as major fault-bounded topographic escarpments with measurable relief exceeding one contour interval of 20m (Wells et al. 1988). The degree of erosional modification of tectonic structures is measured by the mountain front sinuosity index (Bull, 1977a, 1978; Bull and McFadden, 1977; Rockwell et al. 1984; Wells et al. 1988 and Keller and Pinter, 2002 and Silva et al. 2003). This index has been used to evaluate the relative tectonic activity along mountain fronts (Keller and Pinter, 2002 and Silva et al. 2003).

Mountain front sinuosity index Smf (Bull, 2007) is defined as,

$$S_{mf} = \frac{L_{mf}}{L_s} \qquad \textbf{Eq. (1)}$$

The index is defined as;

Where **Smf** = mountain front sinuosity index

Lmf = straight line distance along a contour line

Ls = true distance along the same contour line

The Smf index reflects a balance between the tendency of stream and slope process to produce an irregular (sinuous) mountain front and vertical active tectonics to produce a prominent straight front (Keller, 1986) than mountain fronts in regions where erosion dominates over tectonics.

In active mountain fronts, uplift will prevail over erosional processes, yielding straight fronts with low values of Smf and inactive or less active fronts are marked by irregular or more eroded profiles, with higher Smf values (Wells et al. 1988). Thus, the morphology of a mountain front depends upon the degree of tectonic activity along the front. Some studies have proposed that the lower values of the Smf index (<1.4) are indicative of tectonically active fronts (Keller, 1986), while higher Smf values (>3) values signify relatively less tectonic activity (Bull, 1977b, 1978; Bull and McFadden, 1977; Burbank and Anderson, 2001 and Keller and Pinter, 2002; Wells et al. 1988). Whereas an inactive mountain front may have values as high as 7 (Bull and McFadden,

1977). Smf is widely used geomorphic measure of seismic activity. Typically, earthquakes are concentrated on detached mountain fronts (Keller and Pinter, 2002). In the present study, Smf values are computed for 13 Sub-basins using Lmf and Ls values measured from ASTER GDEM elevation model with a spatial resolution of 30 m and the generated Smf values (Table 5.1 a-m) are categorized according to Bull and McFadden, (1977; Fig. 3.2 and 3.3).

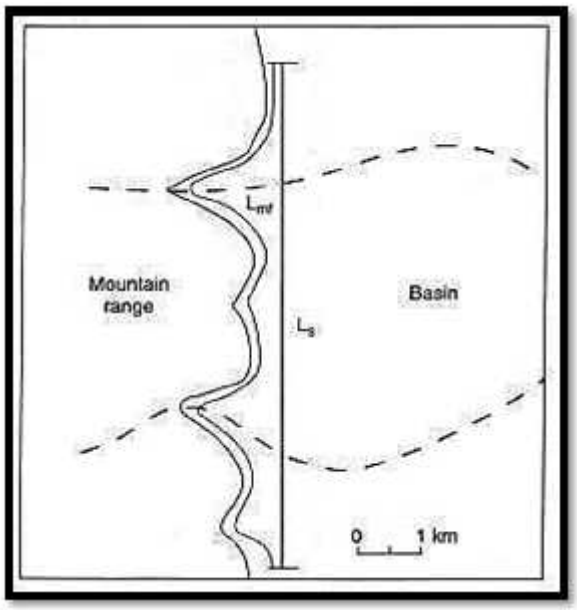

Fig. 3.2 Calculation of mountain front sinuosity (Smf) index (Modified from Keller and Pinter 2002, Fig. 4.14, p. 137).

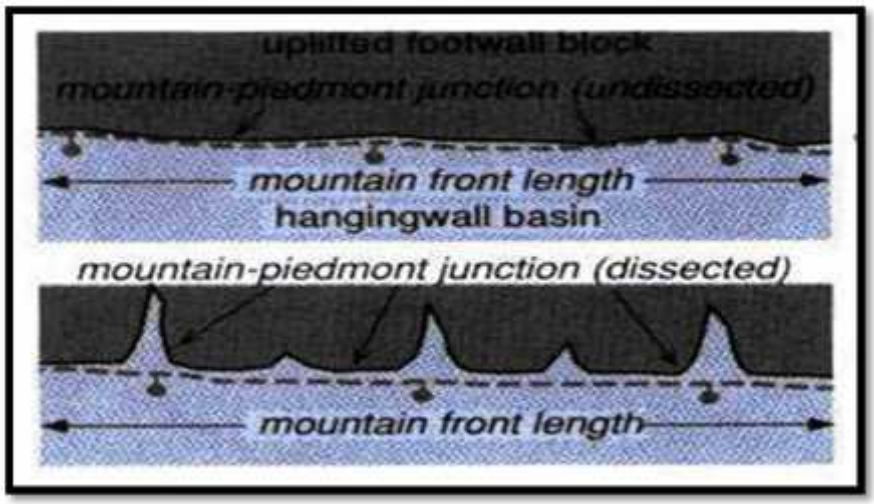

Fig. 3.3 Mountain front sinuosity (Smf) index (Modified from Burbank and Anderson 2001, Fig. 10.5, p. 205).

3.2.4 Basin shape index (Bs)

The typical basin of a tectonically active mountain range is elongate, parallel to the topographic slope of a mountain. The elongated shapes are transformed into circular basins with time, as tectonic activity reduces and continued topographic evolution or upliftment (Bull and McFadden, 1977). The reason of this transformation is because the drainage basin widths are much narrower near the mountain front in tectonically active areas where the energy of the stream has been directed primarily to downcutting. By contrast, a lack of continuing rapid uplift permits widening of the basins upstream from the mountain front. The horizontal projection or planimetric shape of a basin may be described by the basin shape index or the elongation ratio, Bs (Ramirez-Herrera, 1998) or elongation ratio is expressed as:

$$B_s = \frac{B_l}{B_w} \qquad \textbf{Eq. (2)}$$

Where Bl is the length of a basin measured from the headwaters point to the mouth, and Bs is the width of a basin measured at its widest point. High values of Bw are associated with elongated basins, generally associated with relatively higher tectonic activity. Low values of Bs indicate a more circular-shaped basin, generally associated with low tectonic activity. Therefore, Bs may reflect the rate of active tectonics.

3.2.5 Drainage Basin Asymmetry (AF)

Structural control of the orientation of bedding may play a vital role in the growth of basin asymmetry and tilting of bedding allows for preferred migration of the valley in the down-dip direction, producing an asymmetric valley (Cox, 1994), as shown in Fig. 3.4.

In tectonically active topography, the landforms are characterized by relatively steep, mountainous sides and flat floors. The steep sides are created by displacement on faults such that the valley floor moves down relative to the surrounding margins, or, conversely, the margins move up relative to the floor. This movement results in basin tilting and causes the river to migrate latterly and deviate from the basin midline (Hare

and Gardner, 1985 and Keller and Pinter, 2002). The asymmetry factor (AF) enabled to detect tectonic tilting transverse to flow at drainage-basin or larger scales (Hare and Gardner, 1985 and Keller and Pinter, 2002).

The asymmetry factor is determined by the following formula:

$$\mathbf{AF = 100\ (Ar/At)} \qquad \textbf{Eq. (3)}$$

Where **AF**= Asymmetry Factor

Ar = Area of the basin belongs to right (looking downstream) trunk of the Stream

At = Total area of basin

The asymmetry factor (AF) for most stream networks in steady settings is 50. AF significantly greater or smaller than 50 shows influence of active tectonics (tectonic rotation) or lithology control or differential erosion, as for example the stream slipping down bedding plains over time (El Hamdouni et al. 2008). AF is close to 50, if there is no or a little tilting perpendicular to the direction of the trunk channel. Assuming the tectonic activity caused a left dipping to the drainage basin, the tributaries to the left of the main stream will be shorter compared to the ones to the right side of the stream with an asymmetry factor greater than 50, and vice versa (Hare and Gardner, 1985 and Keller and Pinter, 2002).

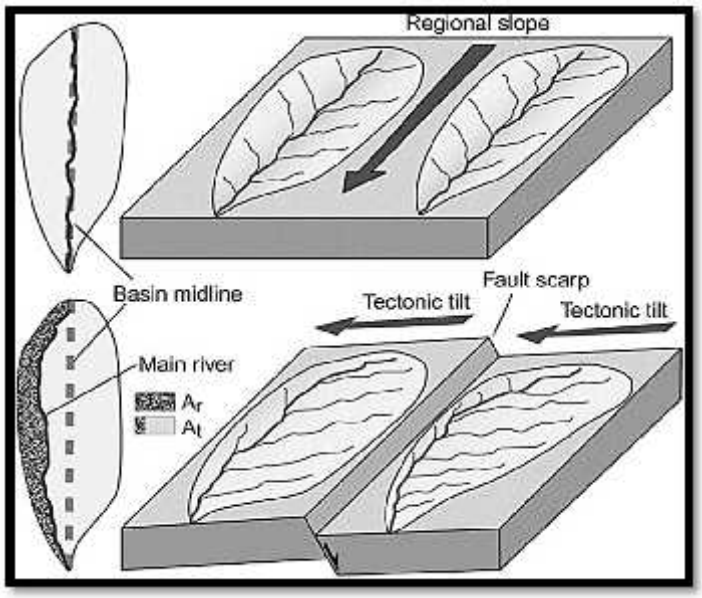

Fig. 3.4 Drainage response to uplift along a fault by migrating laterally in a down-tilt direction, Ar is the area of the basin to the right (looking downstream) of the trunk stream and At is the total area of the drainage basin (modified after Keller and Pinter, 2002 Fig. 4.3, p. 125)

3.2.6 Transverse Topographic Symmetry Factor (*TTF*)

Another quantitative index to evaluate basin asymmetry is the Transverse Topographic Symmetry Factor (*TTF*) that is defined as:

$$TTF = Da / Dd \qquad \text{Eq. (4)}$$

where D_a represents the distance from the midline of the drainage basin to the midline of the active meander belt and D_d corresponds to the distance from the basin midline to the basin divide (Fig.3.5). For diverse segments of valleys, the calculated TTF values indicate migration of streams perpendicular to the drainage-basin axis. Thus, the Transverse Topographic Symmetry Factor is a vector that has direction and magnitude that ranges from zero to one (TTF = 0 to 1), which reflects a perfect asymmetric basin or a tilted one respectively (Cox, 1994; Cox et al. 2001; Burbank and Anderson, 2001 and Keller and Pinter, 2002). As the stream migrates laterally away from the center of the basin and toward one of the two margins, the value of T increases and approaches 1.

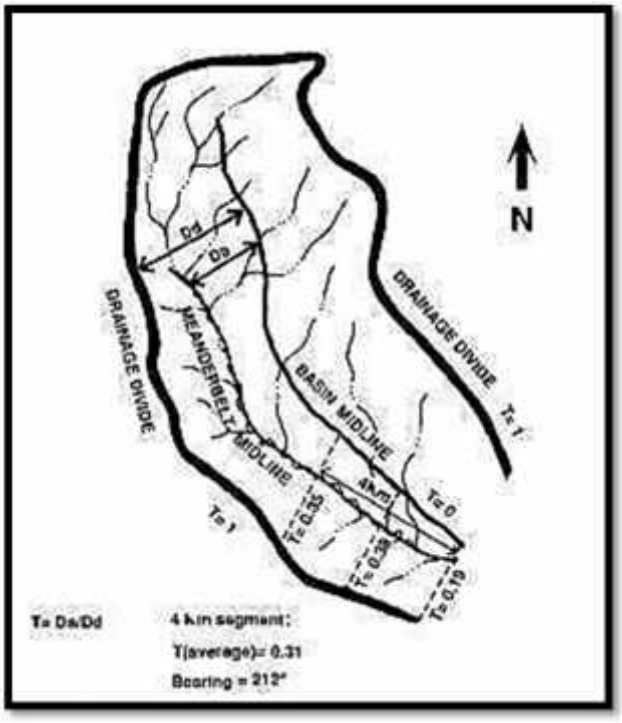

Fig. 3.5 An example of calculating a drainage-basin Transverse Topographic Asymmetry Factor for a single stream segment (From Cox, 1994, Fig. 3, p. 574).

In order to calculate the TTF index, the main stream of the sub-basin was divided into 1 km-long segments. The values of TTF are calculated for each segment and represented as a two-dimensional vector. The length of the vector is equivalent to the ratio Da / Dd, and its direction is perpendicular to the segment of the stream. The vector direction indicates movement of the segment, in the following sense and for the Stream, with regard to the basin midline (Fig. 3.6).

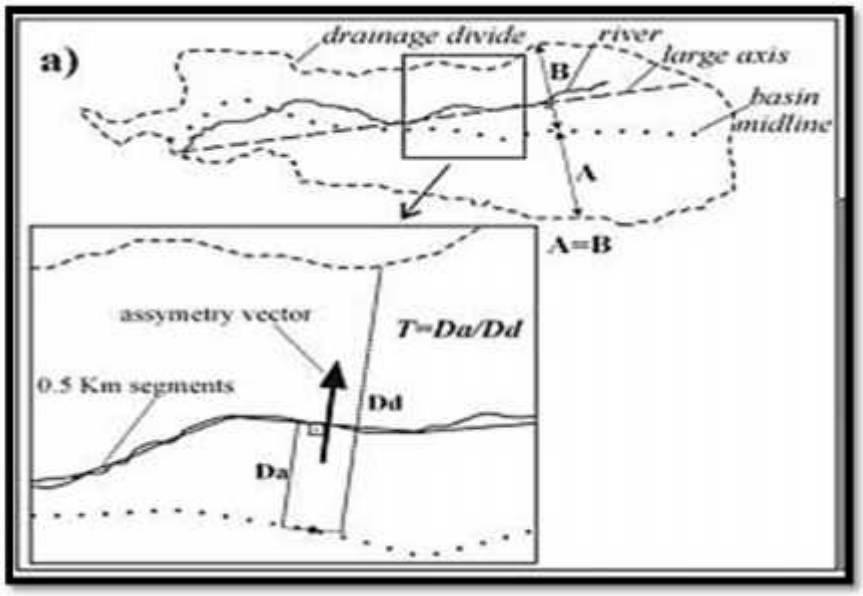

Fig. 3.6 An example of calculating a drainage-basin Transverse Topographic Asymmetry.

In case of a negligible influence by the bedrock tilting on the relocation of the stream channels, the direction of the regional migration is an indicator of the ground tilting in that similar direction. The calculation of both AF and T is a quantitatively rapid method of identifying ground tilting (Cox, 1994; Cox et al. 2001 and Keller and Pinter, 2002).

3.2.7 Hypsometric Integral (HI)

The HI is generally derived for a particular drainage basin and is an index that is independent of basin area. The HI is an index that explains the distribution of elevation of a given area of a landscape, particularly a drainage basin (Strahler, 1952). The index is defined as the area below the hypsometric curve and thus expresses the volume of a basin that has not been eroded. The simple equation that may be used to calculate the index (Mayer, 1990 and Keller and Pinter, 2002) is

$$H_i = \frac{mean\ \text{elevation} - \text{minimum elevation}}{\text{maximum elevation} - \text{minimum elevation}} \qquad \textbf{Eq. (5)}$$

Calculating the hypsometric integral (Hi) is achieved by deriving the maximum and minimum elevation directly from a topographic map. The mean elevation is calculated by obtaining the mean of at least 50 elevation values in the basin using point sampling on a grid (Pike and Wilson, 1971 and Keller and Pinter, 2002) and evaluated directly from the digital elevation model (DEM) of the basin (Pike and Wilson, 1971; Keller and Pinter, 2002; Luo, 2002; Luo and Howard, 2005). HI values of <0.30 describe "tectonically stable", "denuded", "mature" basins according to W.M. Davis (1899) HI values >0.60 indicate "unstable", "actively uplifting", "young" basins. High values of HI generally mean that not as much of the uplands have been eroded, and may propose a younger landscape possibly produced by active tectonics. Low HI values are related to older landscapes that have been more eroded and less impacted by recent active tectonics.

3.2.8 Longitudinal Profile

The Longitudinal Profile is drawn for elevation in y- axis and distance in x-axis (Fig. 3.7). According to (Sinha, 2001), the analysis of longitudinal profile, is the most commonly used technique to identify river response to tectonics. The utility of this parameter is based on the facts that irregularities in channel slope might reflect disequilibrium conditions, suggesting uplift along active faults. Upwardly concave profiles may suggest prolonged basin and channel degradation associated with longer periods of time since basement lowering. More upwardly convex profiles suggest less channel downcutting, continued base-level lowering and/or less time since base-level fall (Wells et al. 1988).

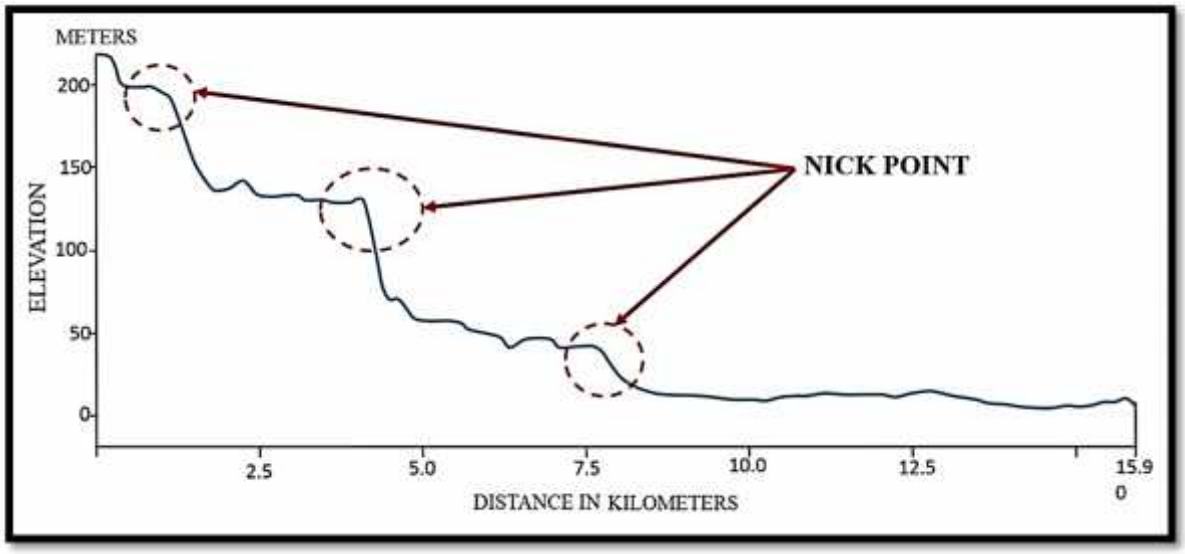

Fig. 3.7 Longitudinal Stream Profile showing Knick Point impacted by tectonic process.

3.3 Geophysical Analysis

3.3.1 Ground Penetrating Radar (GPR)

Ground Penetrating Radar (GPR) is a non-invasive electromagnetic (EM) investigation method for high-resolution detection, rapid imaging and continuous/step mapping of spatial variation in subsurface soils and rock conditions of different dielectric properties. The theory and methodology was adequately explained by (Morey, 1974; Ulriksen, 1982; Davis and Annan, 1989; Beres and Haeni, 1991; Smith and Jol, 1995 and Anon, 1999). In accordance with the laws of classical electromagnetism, as the pulses propagate downwards through the ground, they interact with subsurface materials in a variety of ways which includes attenuation, reflection, refraction, diffraction and scattering (Fig. 3.8). Attenuation caused by the propagation medium and by the path and spreading losses causes the received signal to be significantly diminished in amplitude compared with the transmitted signal. When an EM pulse propagates through a medium, the electric field generated causes electric charges to move by conduction currents and displacement currents (Fig. 3.8)

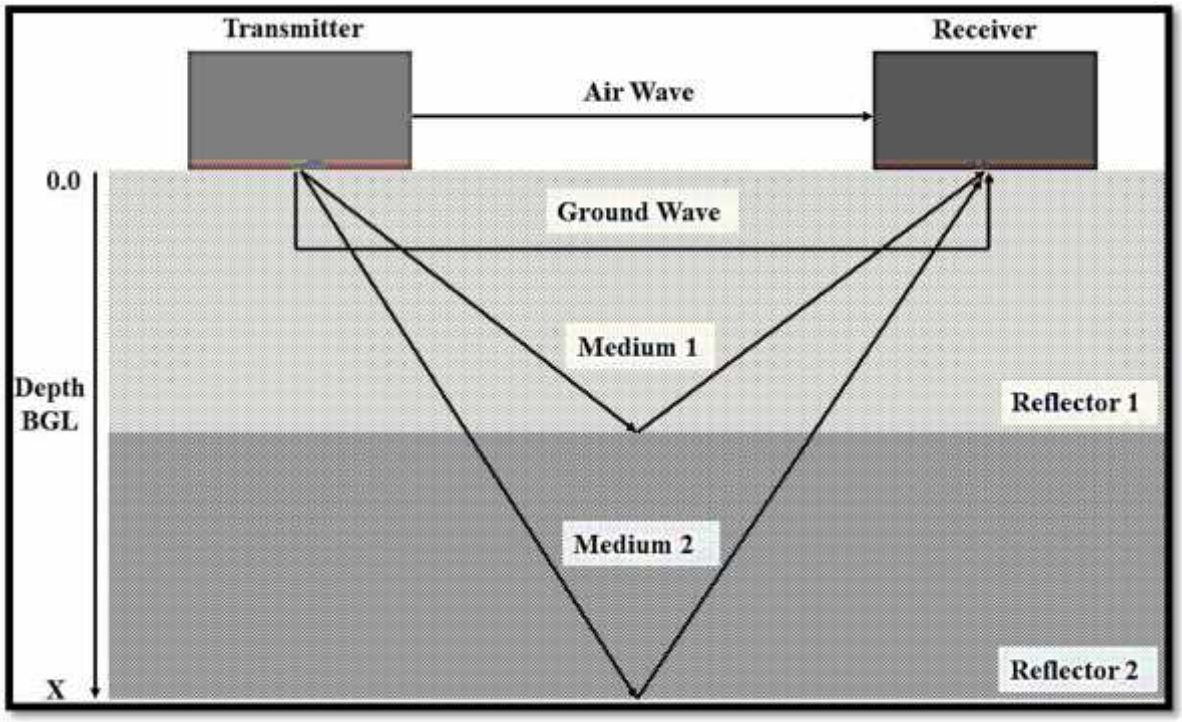

Fig. 3.8 Theoretical principle of EM pathways between transmitter and receiver of a bistatic antenna configuration.

3.3.1.1 GPR Field Survey Method

GPR profiles were conducted along the vicinity of the identified faults to analyse the subsurface structures using the GSSI SIR System-3000 with bistatic multiple low frequency (MLF) Model 3200 center frequency antenna (CFA) and monostatic survey wheel antenna model 5106. The transmission frequency adjusted for bistatic antenna ranges from 80 to 15 MHz on the basis of the depth of interest and the size of the target, while transmission frequency for monostatic survey wheel antenna model is 200 MHz and both antenna models are ground-coupled. The bistatic antennas were placed at a survey point on an established constant grid interval and then moved to the next survey point and so on until the completion of profile while the monostatic antenna was used for continuous GPR profiling using survey wheel method.

In the present study, both the antennas were used for the GPR survey.

3.3.1.2 GPR Data Processing and Interpretation

A GPR display typically consists of a collection of time-series returns viewed stacked side- by-side giving a depth profile of the subsurface. The collected GPR field data has been processed and analysed by a combination of automated and manual processing sequence by using GSSI RADAN 6.6 software. Various data editing and processing techniques involves complex geophysical inversion algorithms like stretching, stacking, zero time adjust, remove out clutters, data filtering, deconvolution, forward modelling or iterative migration, data transformation, velocity analysis and other interactive interpretation as given by GSSI, (2008) were adopted. If the subsurface is perfectly homogeneous, the GPR unit would not record any reflections. Thus, the fact that the earth is heterogeneous gives us radar reflection data to interpret the subsurface conditions. Interpretation of GPR profile have been made through various GPR signal processing techniques and the processed GPR profiles images represented several typical strong, medium and poor reflection amplitudes of subsurface and appears nearly continuous and as a horizontal layer. The GPR reflections with changes in dielectric constant, which in turn are related to changes in soil or rock bedding, buried objects, geological intrusive, void space, fractures, clay type, and fluid content. On the basis of deflection type and amplitude, the GPR image yielded three to five distinct horizontal layers that varies in thickness because of subsurface geological characteristics.

GPR produces a time-distance record of the subsurface and these signatures can be plotted as 2D profiles, 3D models and plan view image of successive traces of waveforms of different depths. These waveforms can either be displayed in a “wiggle form” plot, or “colour-coded” plot by representing each waveform by a vertical line with the amplitude of each sample represented by a pixel intensity level or colour (Fig. 3.9). In GPR profile, the horizontal scale represents units (Meters) of distance travelled along a grid line. The vertical scale is time (ns) or depth (meters) scale. The subsurface geological features such as folds, faults/fractures of the processed data were interpreted on the basis of the host materials and the reflection configurations as depicted in Fig. 3.10.

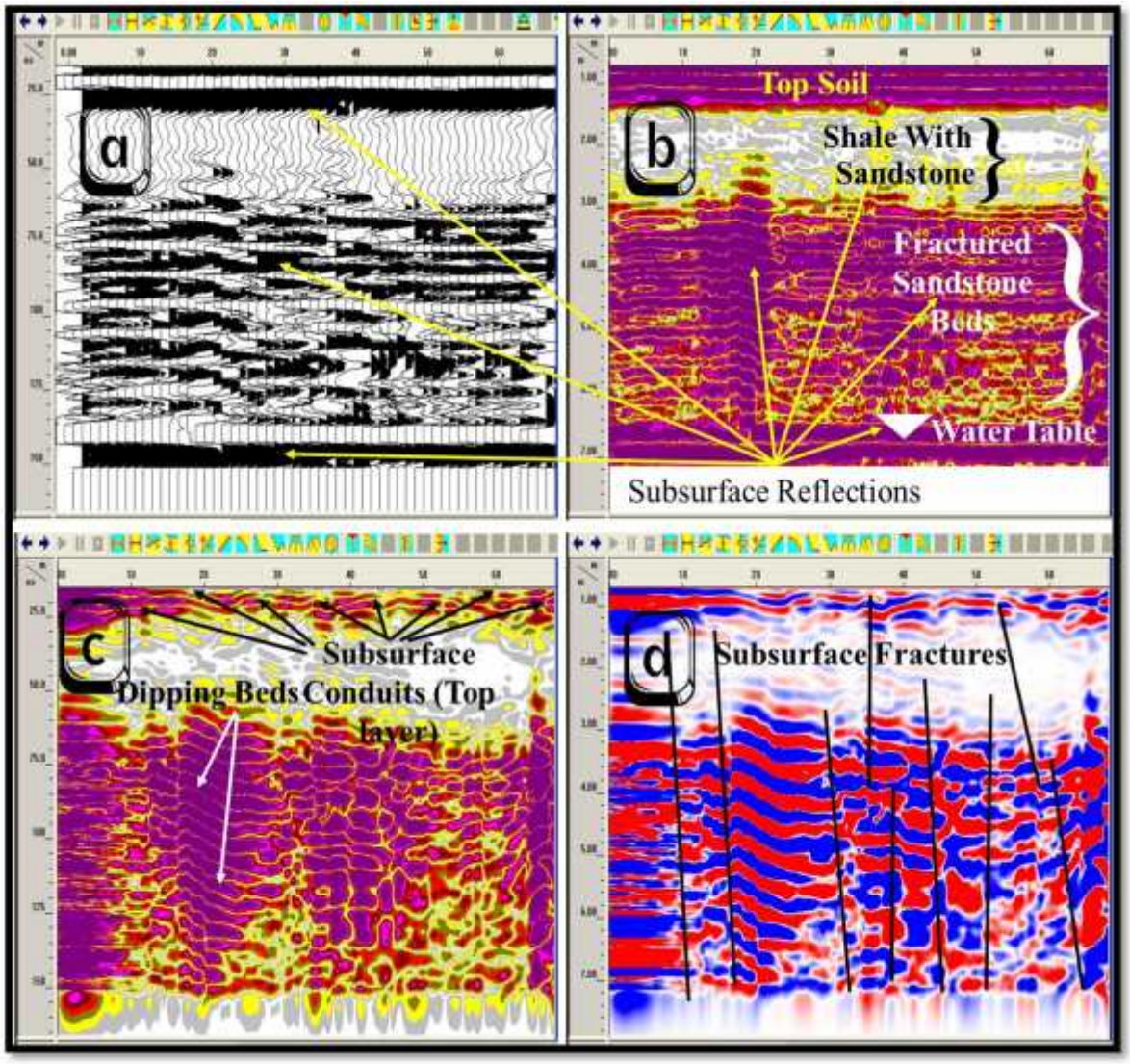

Fig. 3.9 GPR profile image of South Point showing (a) wiggle trace format and processed and interpreted images (b, c and d) using RADAN software.

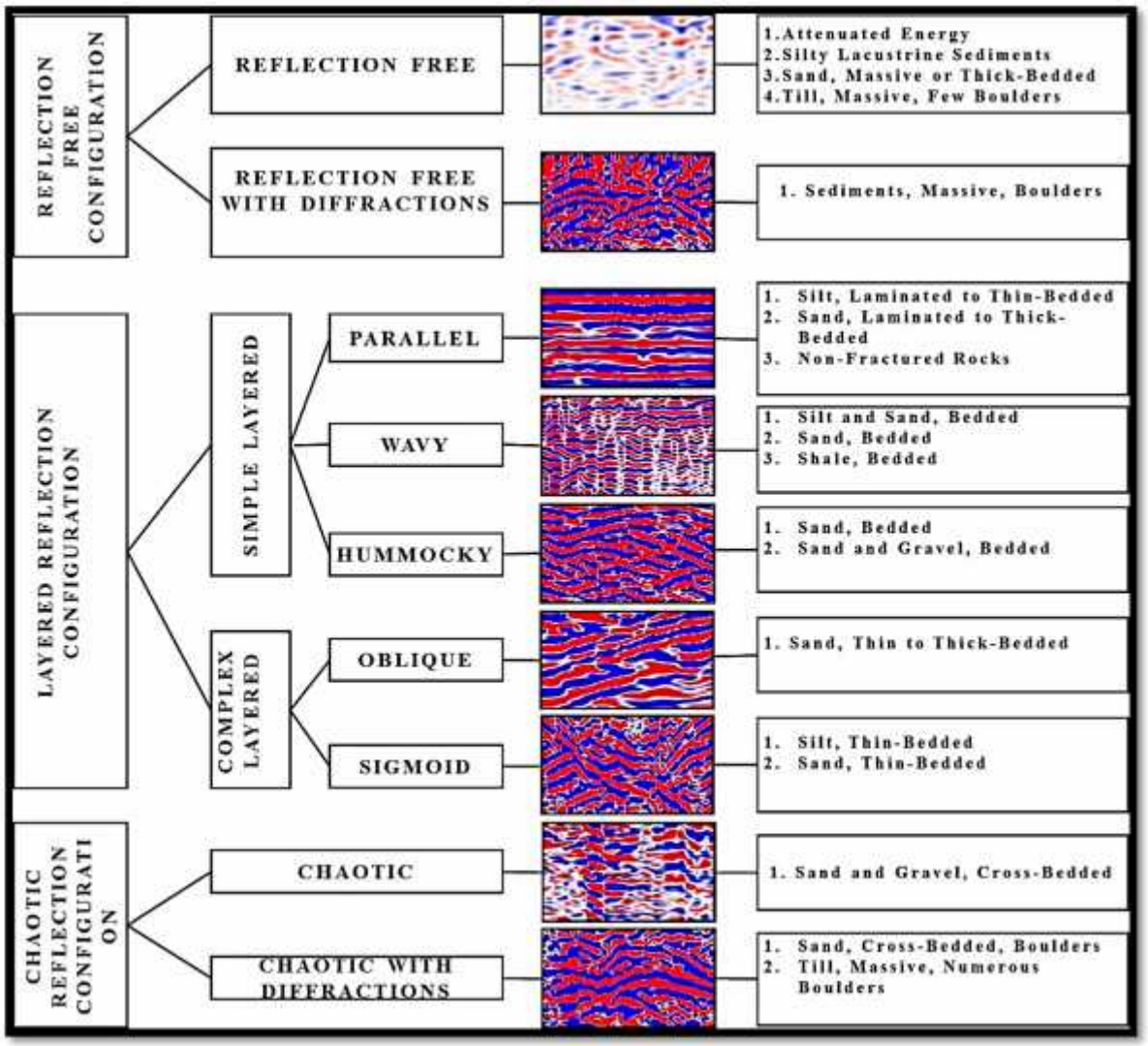

Fig. 3.10 Chart relating the reflection configurations on the radar record to the lithologic and stratigraphic properties of subsurface of South Andaman Island (modified after Beres and Haeni, 1991).

3.4 Seismotectonic Analysis

3.4.1 Power law and G-R relation

Earthquakes are not uniformly distributed in space, time and magnitude. Earthquake distribution spatial patterns and temporal patterns of occurrence were demonstrated to be fractal. Distribution of earthquakes with respect to magnitudes exhibits scale invariability, appears to be self-similar and obeys a power law or fractal scaling. Many complex space-time phenomena, such as seismicity may be interpreted in terms of fractal distributions with power-law scaling (Hirata, 1989; Oncel et al. 1995; Caneva and Smirnov, 2004; Oncel and Wilson, 2007 and Roy et al. 2011).

The power law is:

$$\mathbf{P\ (t_w) \propto (t_w)^{\alpha}}$$ (Schonfelder et al. 2006)

P (t_w) is the probability distribution time of the event. $(t_w)^{\alpha}$ is the exponential waiting time and It follows the straight log-log coordinates. Shorter waiting time deviates from the power law. Japanese believe that all fault displacements are self-similar and the areas of faults also follow Power law.

The fractal distribution of epicentres of earthquakes implies the absence of a characteristic event size (theoretical limits on the maximum earthquake size). An empirical formula

$$\mathbf{\log N = a - bM} \qquad \textbf{Eq. (1)}$$

$$\mathbf{N = 10^{a - bM}}$$

is known in the east as Ishimoto and Iida, (1939) relation and in the west as the Gutenberg and Richter (G-R) relation which advocates that the frequency of earthquake occurrence in a given area during a specific period of observation can be expressed as a function of magnitude. (Gutenberg and Richter, 1944)

N refers to a number of events with magnitudes equal to or larger than M with magnitude, M, where 'a' and 'b' are positive, real constants. 'a' describes the seismic activity (log number of events with M=0). It is determined by the event rate and for certain region depends upon the volume and time window considered. b, which is typically close to 1, is a tectonic parameter describing the relative abundance of large to smaller shocks. It seems to represent properties of the seismic medium in some respect, like stress and/or material conditions in the focal region. The parameter 'a' shows the activity level of seismicity and exhibits significant variations from region to region. It also depends on the period of observation and the size of area of investigation. The parameter 'b' is related to tectonic structure and depends upon the stress regime of the studied region (Hatzidimitriou et al. 1985; Tsapanos, 1990; Al-Amri and Punsalan, 1998 and Schorlemmer et al. 2005).

High and low stresses cause earthquake series with low and high b-values respectively (Scholz, 1968 and Wyss, 1973). This observation is employed to study stress levels and structural anomalies in the crust and/or upper mantle (subduction) e.g. in earthquake prediction, identifying volumes of active magma bodies (Wiemer and Benoit, 1996; Wiemer at al., 1998) or roots of regional volcanism (Monterroso and Kulhanek, 2003) and material heterogeneity (Mogi, 1962). It is noted that large heterogeneities correspond to higher b-values. Therefore, the estimation of 'b' value is important in earthquake prediction. In order to calculate the b-value, earthquake parameters have been collected through various sources viz IMD, USGS catalogue, ISC and CMD catalogue from 1918 to 2013. The epicenter location of various tremors has been plotted in SRTM satellite imagery. The 'b' value for the different seismogenic region viz A to E was calculated by using G-R relation.

In the present study, the minimum denomination of the magnitude (ΔM) is equal to 0.1 while estimating 'b' value which have large span of earthquakes 5.0 to 8.6 magnitude. The cutoff magnitude Mc has been detected while estimating the b-value with eye judgment from the plot. The minimum body wave magnitude considered is greater than or equal to critical magnitude (Mc). i.e. ($Mb \geq Mc$).